nature portfolio

https://doi.org/10.1038/s41586-023-06441-6

Supplementary information

Structural mechanism of mitochondrial membrane remodelling by human OPA1

In the format provided by the authors and unedited

Figure 2f:

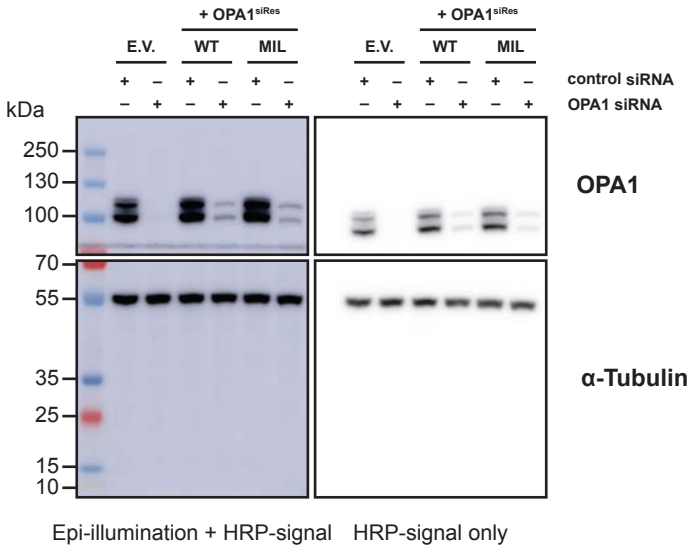

Figure 3d:

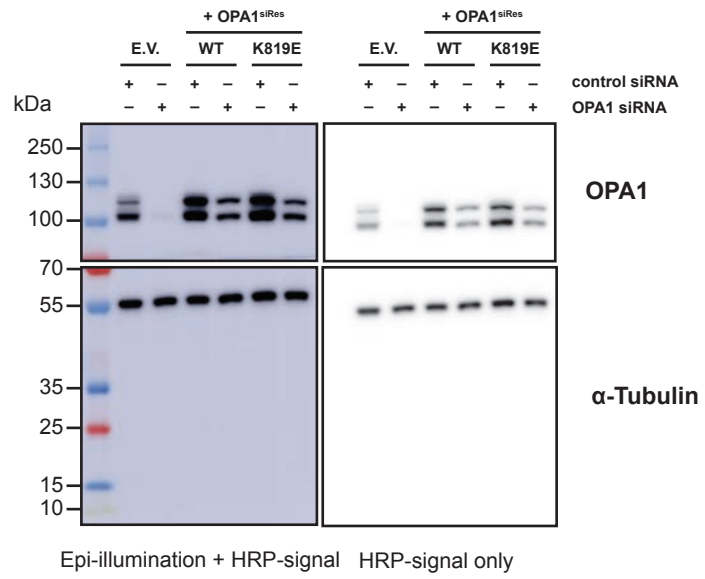

Extended Data Figure 1b:

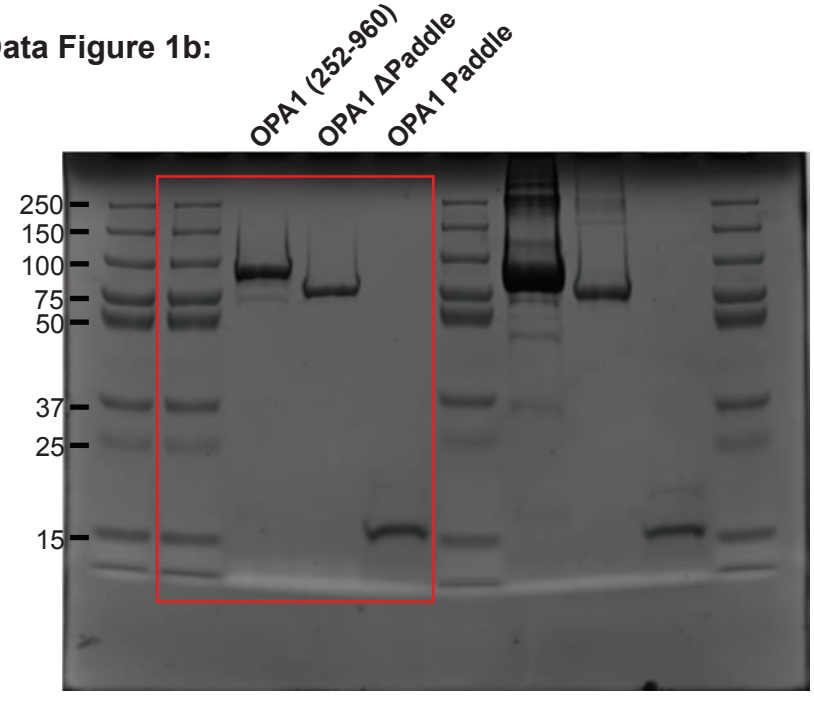

Extended Data Figure 7a:

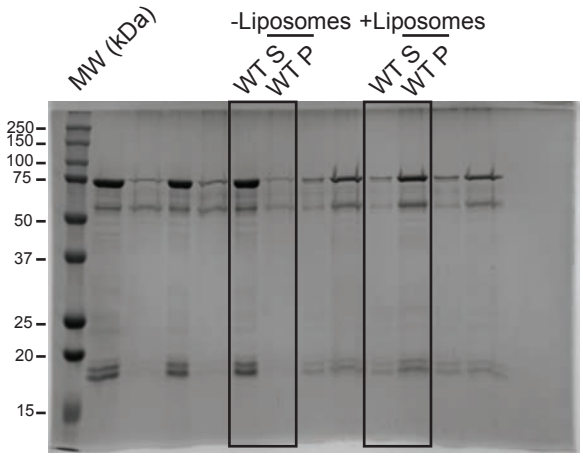

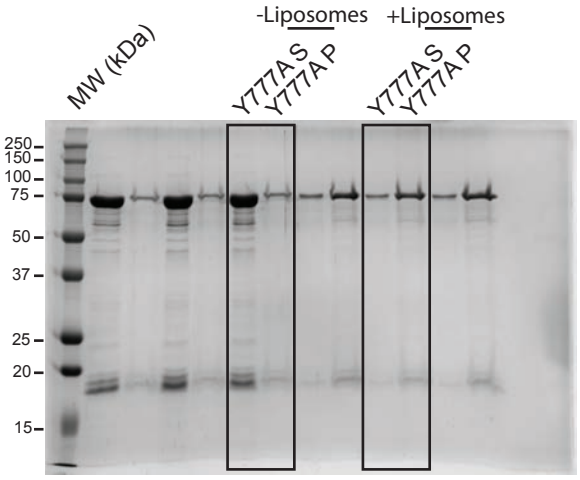

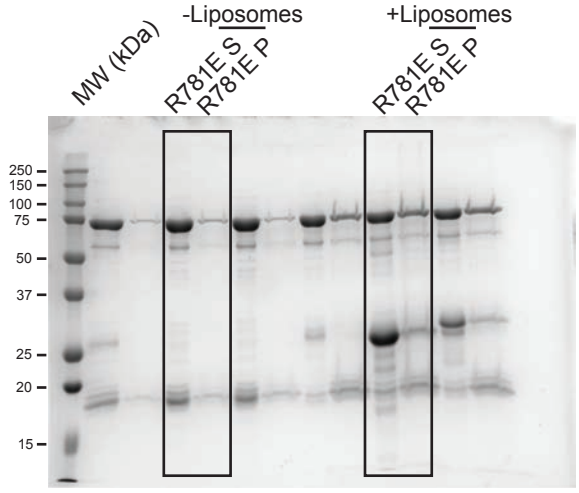

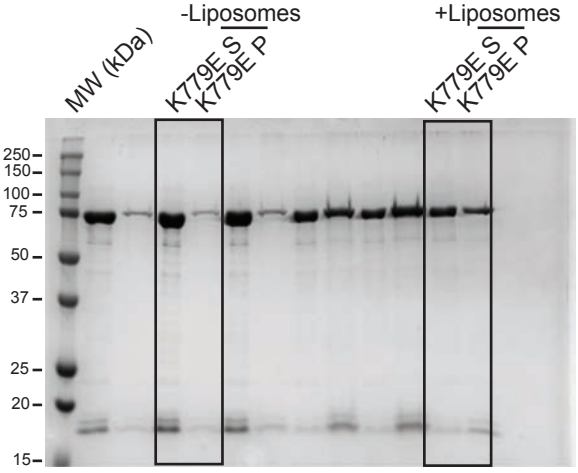

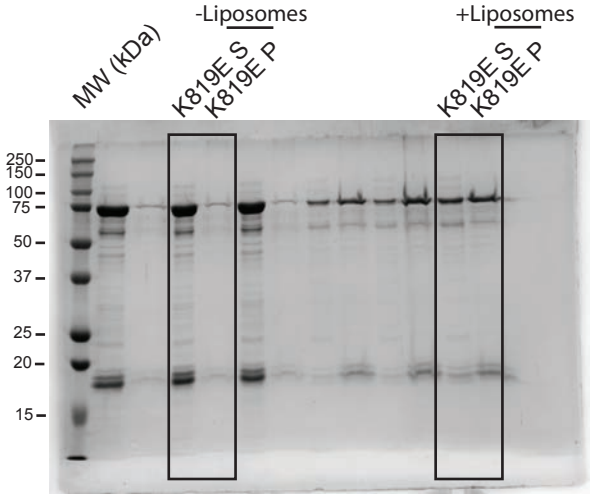

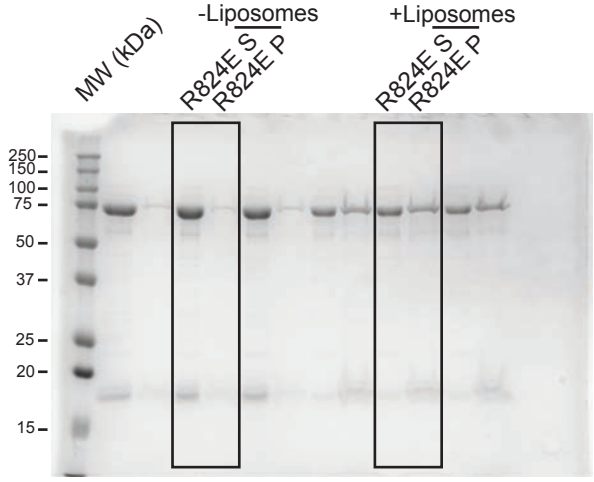

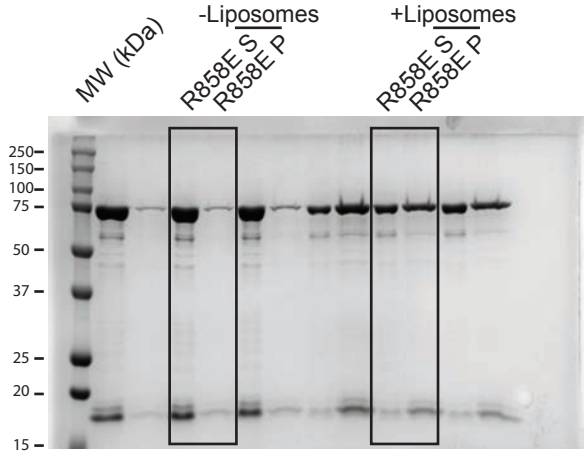

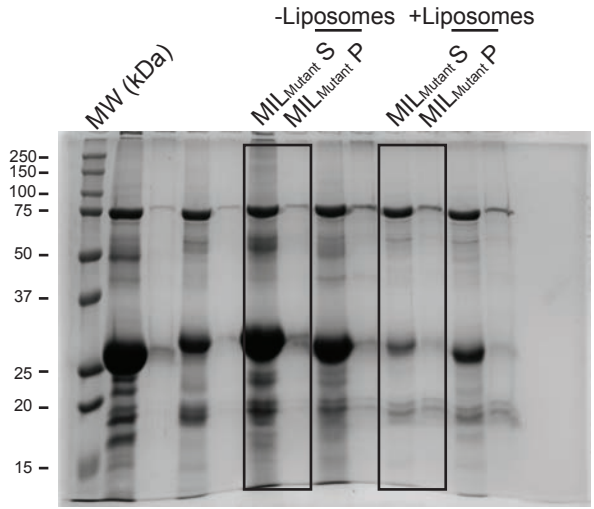

Extendet Data Figure 8b:

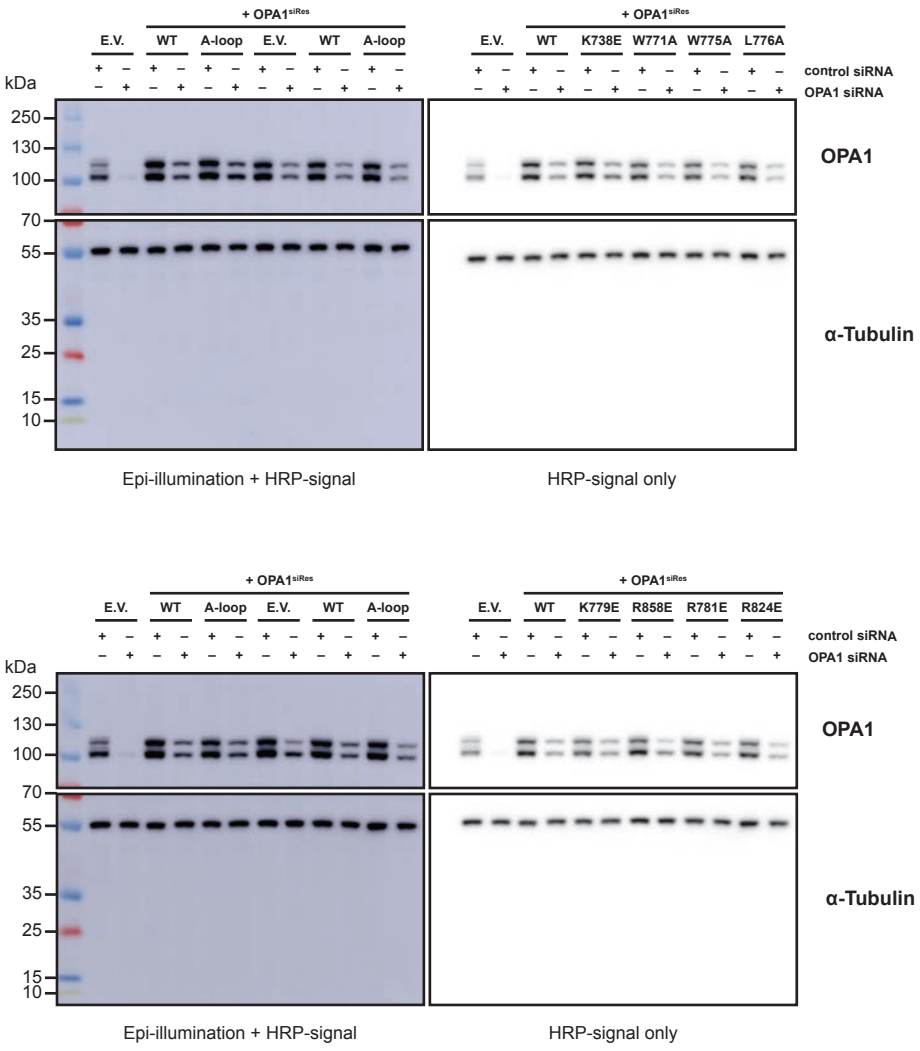

Supplementary Figure 2:

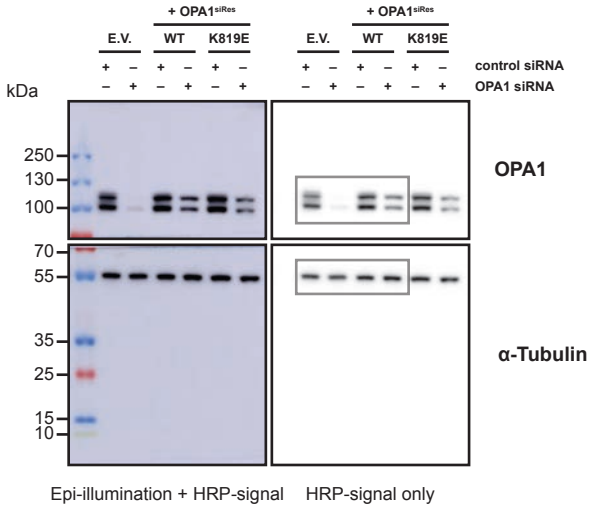

Supplementary Figure 3:

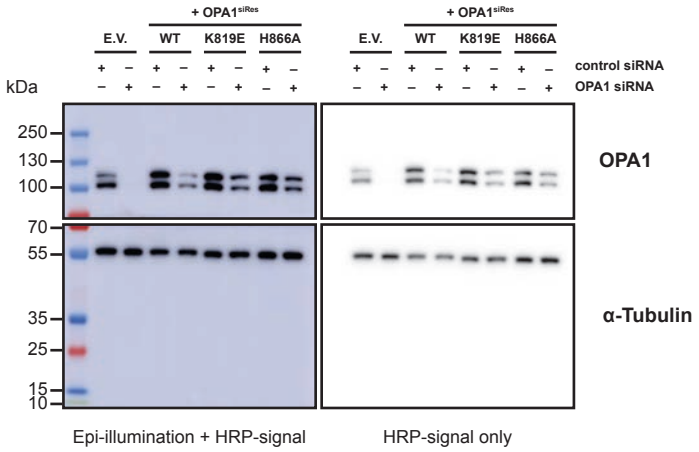

Supplementary Figure 1. Raw Gels from Figure 2f, Figure 3d, Extended Data Figure 1b, Extended Data Figure 7a, Extended Data Figure 8b, Supplementary Figure 2, and Supplementary Figure 3.

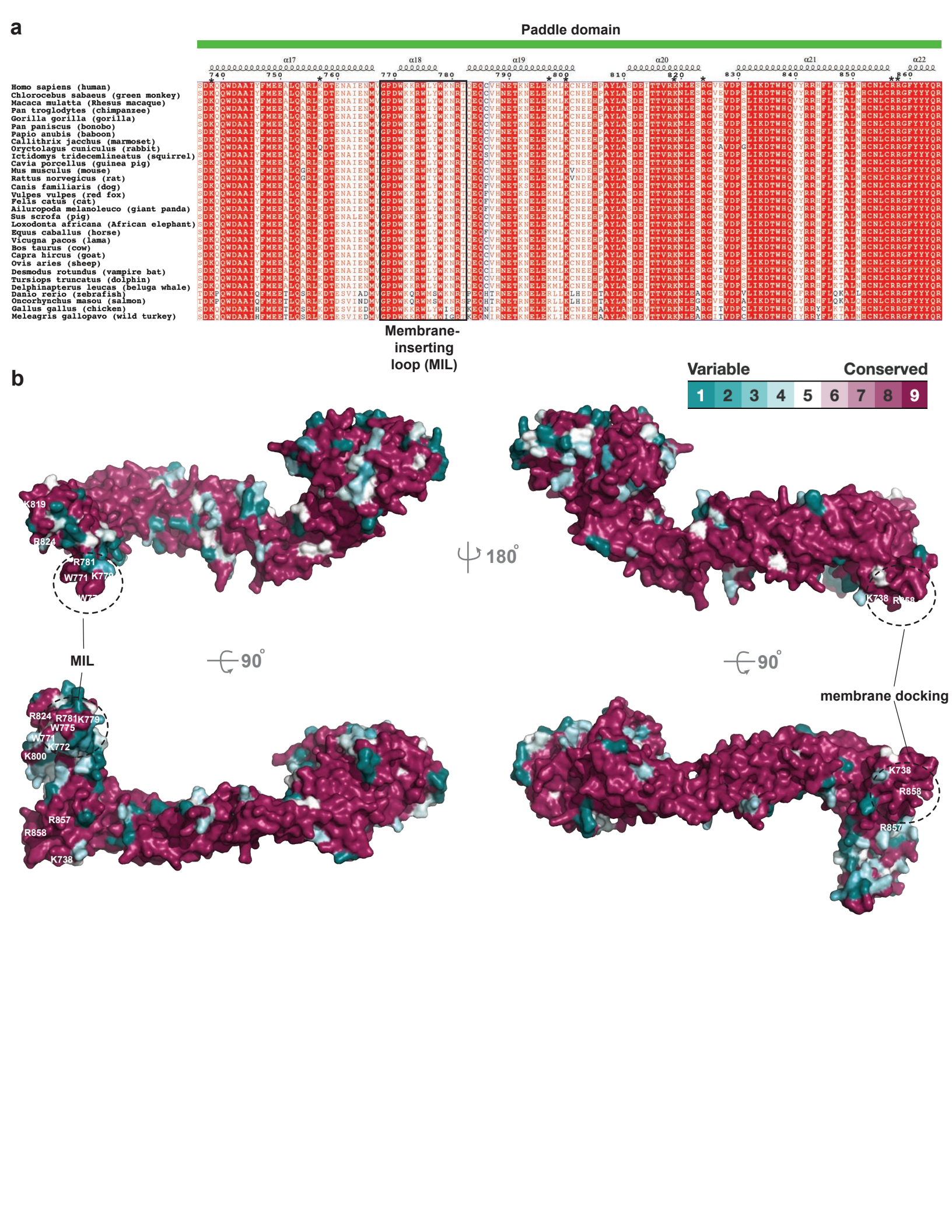
a
Paddle domain
α17
α18
α19
α20
α21
α22
740
750
760
770
780
790
800
810
820
830
840
850
860
Homo sapiens (human)
Chlorocebus sabaeus (green monkey)
Macaca mulatta (Rhesus macaque)
Pan troglodytes (chimpanzee)
Gorilla gorilla (gorilla)
Pan paniscus (bonobo)
Papio anubis (baboon)
Callithrix jacchus (marmoset)
Oryctolagus cuniculus (rabbit)
Ictidomys tridecemlineatus (squirrel)
Cavia porcellus (guinea pig)
Mus musculus (mouse)
Rattus norvegicus (rat)
Canis familiaris (dog)
Vulpes vulpes (red fox)
Felis catus (cat)
Ailuropoda melanoleuco (giant panda)
Sus scrofa (pig)
Loxodonta africana (African elephant)
Equus caballus (horse)
Vicugna pacos (lama)
Bos taurus (cow)
Capra hircus (goat)
Ovis aries (sheep)
Desmodus rotundus (vampire bat)
Tursiops truncatus (dolphin)
Delphinapterus leucas (beluga whale)
Danio rerio (zebrafish)
Oncorhynchus masou (salmon)
Gallus gallus (chicken)
Meleagris gallopavo (wild turkey)
Membrane-inserting loop (MIL)
b
Variable
Conserved
1
2
3
4
5
6
7
8
9
K819
R824
R781
W771
K772
180°
K738
R858
MIL
90°
90°
membrane docking
R824
R781
K779
W775
W771
K772
K800
R857
R858
K738
K738
R858
R857

Supplementary Figure 2. Conservation of human S-OPA1 paddle domain residues involved in membrane binding and remodeling. a, Multiple sequence alignment (MSA) shows the conservation of S-OPA1 paddle domain residues. Secondary structural elements observed in the cryoEM structure of membrane-bound S-OPA1 are shown as coils for α -helices. Residues that form the membrane-inserting loop (MIL) are highlighted with a black box. Other membrane-interacting or interface residues are highlighted with an asterisk. Red boxes indicate the complete conservation of a given amino acid within the paddle domain. OPA1 sequences from Homo sapiens (human;Uniprot: O60313), Chlorocebus sabaeus (green monkey; Uniprot: A0A0D9R952), Macaca mulatta (rhesus macaque; Uniprot: F6Y1N8), Pan troglodytes (Chimpanzee; Uniprot: A0A2I3SKT2), Gorilla gorilla (gorilla; Uniprot: G3S1U3), Pan paniscus (bonobo; Uniprot: A0A2R9BDG8), Papio anubis (baboon; Uniprot: A0A096N399), Callithrix jacchus (marmoset; Uniprot: A0A2R8PC53), Oryctolagus cuniculus (rabbit; Uniprot: G1TAB7), Ictidomys tridecemlineatus (squirrel; Uniprot: I3MI89), Cavia porcellus (guinea pig; Uniprot: H0V6M3), Mus musculus (mouse; Uniprot: P58281), Rattus norvegicus (rat; Uniprot: Q2TA68), Canis familiaris (dog, Uniprot: F1PK93), Vulpes vulpes (red fox, Uniprot: A0A3Q7T0T6), Felis catus (cat; Uniprot: A0A337SN50), Ailuropoda melanoleuco (cat; Uniprot: G1MBN4), Sus scrofa (pig; Uniprot: A0A5G2QQR2), Loxodonta africana (African elephant; Uniprot: G3SNG0), Equus caballus (horse; Uniprot: F6Z2C8), Vicugna pacos (lama; Uniprot: A0A6I9I1B0), Bos taurus (cow; Uniprot: E1BBC4), Capra hircus (goat; Uniprot: A0A452EKR4), Ovis aries (sheep; Uniprot: A0A6P7D299), Desmodus rotundus (Vampire bat; Uniprot: K9J3D6), Tursiops truncatus (dolphin; Uniprot: A0A2U4ACH9), Delphinapterus leucas (beluga whale; Uniprot: A0A2Y9MT19), Danio rerio (zebrafish; Uniprot: Q5U3A7), Oncorhynchus masou (salmon; Uniprot: O93248), Gallus gallus (chicken; Uniprot: Q5F499), and Meleagris gallopavo (wild turkey; Uniprot: G3UT81), are aligned. **b,** The evolutionary conservation of amino acid positions in OPA1. The conservation analysis was performed using the alignment of all OPA1 sequences, and the conservation of amino acid positions was calculated using the ConSurf server. The conservation scores of surface residue are indicated in a colored gradient from most conserved (burgundy) to least conserved (cyan). As anticipated, the analysis revealed that the S-OPA1 paddle domain is highly conserved.

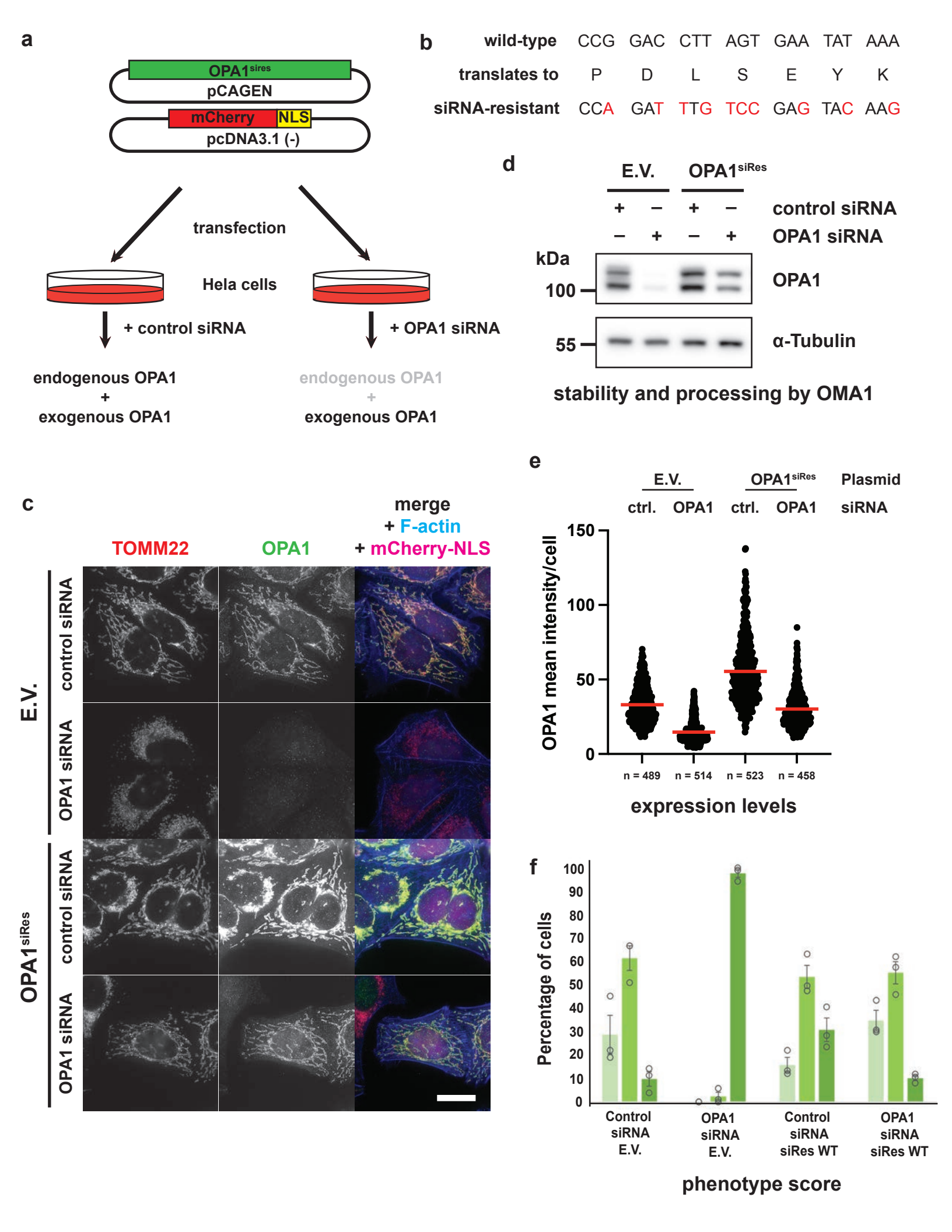
a
OPA1sires
pCAGEN
mCherry
NLS
pcDNA3.1 (-)
transfection
Hela cells
+ control siRNA
+ OPA1 siRNA
endogenous OPA1
+
exogenous OPA1
endogenous OPA1
+
exogenous OPA1
b
wild-type CCG GAC CTT AGT GAA TAT AAA
translates to P D L S E Y K
siRNA-resistant CCA GAT TTG TCC GAG TAC AAG
d
E.V.
OPA1siRes
control siRNA
OPA1 siRNA
kDa
100
OPA1
55
α-Tubulin
stability and processing by OMA1
c
TOMM22
OPA1
merge
+ F-actin
+ mCherry-NLS
E.V.
control siRNA
OPA1 siRNA
OPA1siRes
control siRNA
OPA1 siRNA
e
E.V.
OPA1siRes
Plasmid
ctrl.
OPA1
ctrl.
OPA1
siRNA
OPA1 mean intensity/cell
150
100
50
0
n = 489
n = 514
n = 523
n = 458
expression levels
f
Percentage of cells
100
90
80
70
60
50
40
30
20
10
0
Control siRNA E.V.
OPA1 siRNA E.V.
Control siRNA siRes WT
OPA1 siRNA siRes WT
phenotype score

Supplementary Figure 3. Summary of experimental design and controls used for the cell-based assays. a, The experimental strategy of the OPA1 rescue. Hela cells were transfected with either empty vector (E.V.) or siRNA-resistant OPA1 (mutated sequence illustrated in **b.**) After 24 h, the cells were transfected with control (ctrl.) or OPA1 siRNA for another 72 h. The cells were analyzed by western blot or fluorescence microscopy. **c,** Example pictures of treated Hela cells stained for TOMM22 (red), OPA1 (green), mCherry (magenta), and F-actin (blue). Transfected cells were identified by the nuclear mCherry signal (Bar=20 µm). **d,** Western blot analysis of lysates derived from transfected Hela cells. The blot shows endogenous OPA1 levels (lane 1), knock-down efficacy (lane 2), combined expression of endogenous and exogenous OPA1 (lane 3), and expression levels of mostly exogenous protein. This approach allows the analysis of protein stability and the processing by OMA1 in the intermembrane space. **e,** Quantification of OPA1 expression. Regions of interest were defined by the F-actin stain (cell body) and the mean fluorescent intensity for the OPA1 stain was determined and plotted in a violin graph. Each dot represents the signal obtained from one cell. Both knockdown and overexpression were clearly detectable while the expression of exogenous, siRNA-resistant OPA1 closely resembles endogenous levels. **f,** Quantification of microscopy images of wild-type, empty vector (E.V.), and mutants. Mitochondrial phenotypes observed in HeLa cells transiently expressing human OPA1 variants as described in **(a)** The average percentage of cells belonging to each of three morphological classifications across three experimental replicates. Cells expressing the control siRNA E.V. (n=539 cells), OPA1 siRNA E.V. (n=513 cells), control siRNA WT OPA1 (n=687 cells), and OPA1 siRNA WT OPA1 (n=537 cells) over three experimental replicates. Data points represent average percentage of cells across three experimental replicates. Error bars indicate s.e.m.

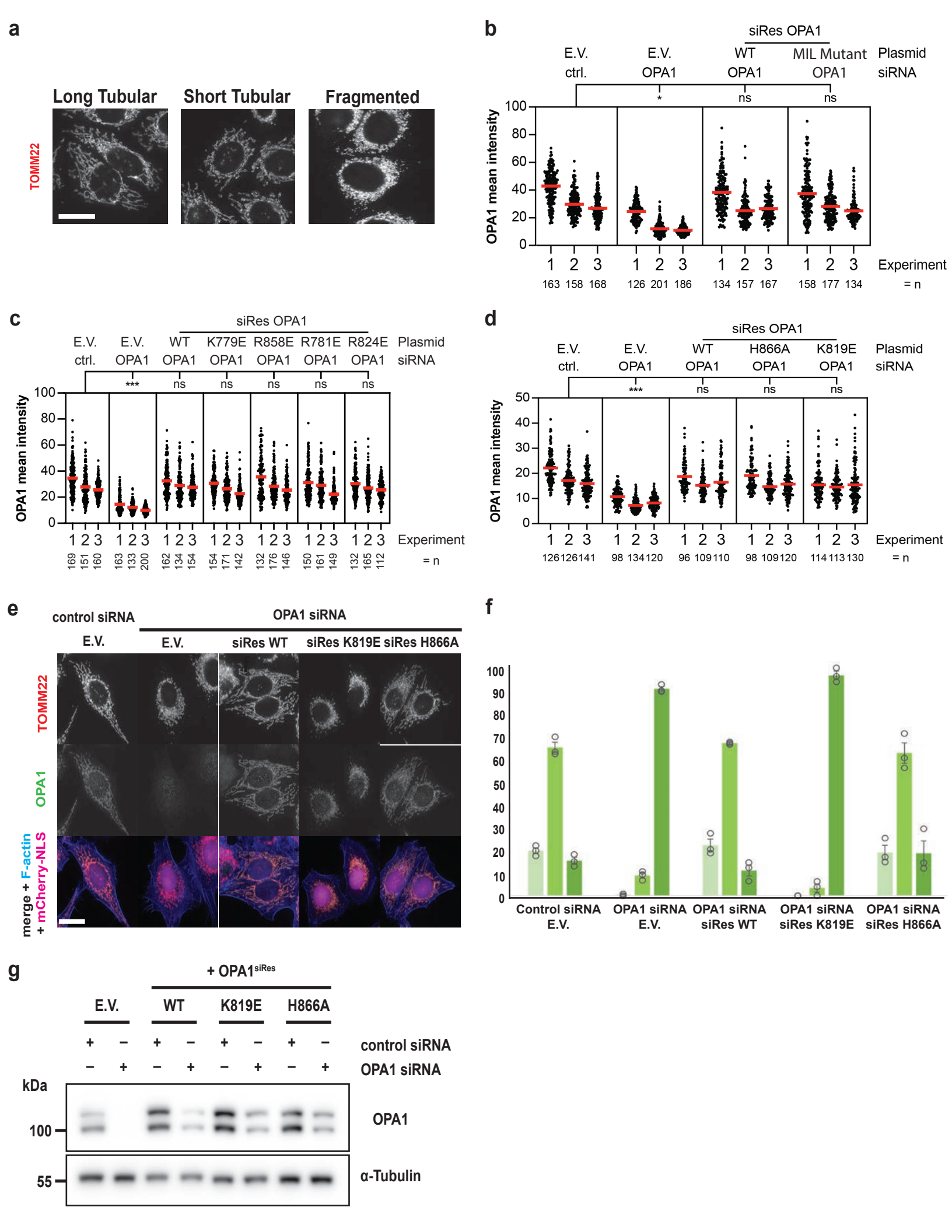
a
Long Tubular
Short Tubular
Fragmented
TOMM22
b
siRes OPA1
E.V. ctrl.
E.V. OPA1
WT OPA1
MIL Mutant OPA1
Plasmid siRNA
*
ns
ns
OPA1 mean intensity
Experiment
= n
163 158 168
126 201 186
134 157 167
158 177 134
c
siRes OPA1
E.V. ctrl.
E.V. OPA1
WT OPA1
K779E OPA1
R858E OPA1
R781E OPA1
R824E OPA1
Plasmid siRNA
***
ns
OPA1 mean intensity
Experiment
= n
169 151 160
163 133 200
162 134 154
154 171 142
132 176 146
150 161 149
132 165 112
d
siRes OPA1
E.V. ctrl.
E.V. OPA1
WT OPA1
H866A OPA1
K819E OPA1
Plasmid siRNA
***
ns
OPA1 mean intensity
Experiment
= n
126 126 141
98 134 120
96 109 110
98 109 120
114 113 130
e
control siRNA
OPA1 siRNA
E.V.
E.V.
siRes WT
siRes K819E
siRes H866A
TOMM22
OPA1
merge + F-actin + mCherry-NLS
f
Control siRNA E.V.
OPA1 siRNA E.V.
OPA1 siRNA siRes WT
OPA1 siRNA siRes K819E
OPA1 siRNA siRes H866A
g
+ OPA1siRes
E.V.
WT
K819E
H866A
control siRNA
OPA1 siRNA
kDa
100
55
OPA1
α-Tubulin

Supplementary Figure 4. Detailed analyses of OPA1 expression in transfected HeLa cells.

a, Representative fluorescent microscopy images of cells showing three different types of mitochondrial network morphology used for manual scoring. Scale Bar, 20 µm. **b-d,** Quantification of OPA1 intensities in cells. Regions of interest were defined based on the F-actin stain and the mean fluorescent intensity of the OPA1 staining within was quantified and visualized in a violin graph in which each dot represents the signal from one cell. The derived numbers are arbitrary and depend on cell density and the staining efficiency (the same microscope settings were used for each experiment). Each experiment was blotted separately. MIL; membrane-inserting loop. To achieve Gaussian distribution, the obtained datasets were log-transformed, and the resulting values were analyzed in a nested one-way ANOVA. b: p value = 0.0268 (*). c: p value = 0.0011 (***). d: p value = <0.0001 (****). (ns = not significant, *≤0.0332, ***≤0.002) **e,** Representative images of cells used for the analysis. HeLa cells were transfected with the indicated plasmids and siRNAs. After fixation, the cells were stained with antibodies that detect TOMM22 (red, mitochondria) and OPA1 (green, detection of expression). Only mCherry-NLS (magenta, transfection control) expressing cells were included in the analysis. To visualize the borders of the cells, an F-Actin stain (Phalloidin-Alexa405, blue) was included in the staining process. Scale Bar, 20 µm **f,** Quantification of microscopy images of empty vector (E.V.), wild-type, and mutants. Mitochondrial phenotypes observed in HeLa cells transiently expressing human OPA1 variants as described in e. The average percentage of cells belonging to each of the three morphological classifications across three experimental replicates. Cells expressing the control siRNA E.V (n=507 cells), OPA1 siRNA E.V. (n=486 cells), wild-type OPA1 experimental (n=363 cells), OPA1 K819E (n=426 cells), and OPA1 H866A (n=407 cells) over three experimental replicates. Error bars indicate s.e.m. **g,** Stability and OMA1 processing of OPA1 mutants. Immunoblot analysis of the corresponding samples. Lane 1 (E.V., ctrl. siRNA) shows the endogenous expression levels of OPA1 in HeLa cells. Lane 2 (E.V., OPA1 siRNA) the knock-down efficacy. Lanes 3, 5, and 7 illustrate the overexpression of OPA1 (endogenous and exogenous) when the transfected cells were treated with control siRNA. The detected OPA1 in lanes 4, 6, and 8 resembles mostly the remaining exogenous siRNA-resistant OPA1 expressed from the plasmids. All tested mutants are stable when compared to the siRNA-resistant WT and processing by OMA1 appears unaltered.

a

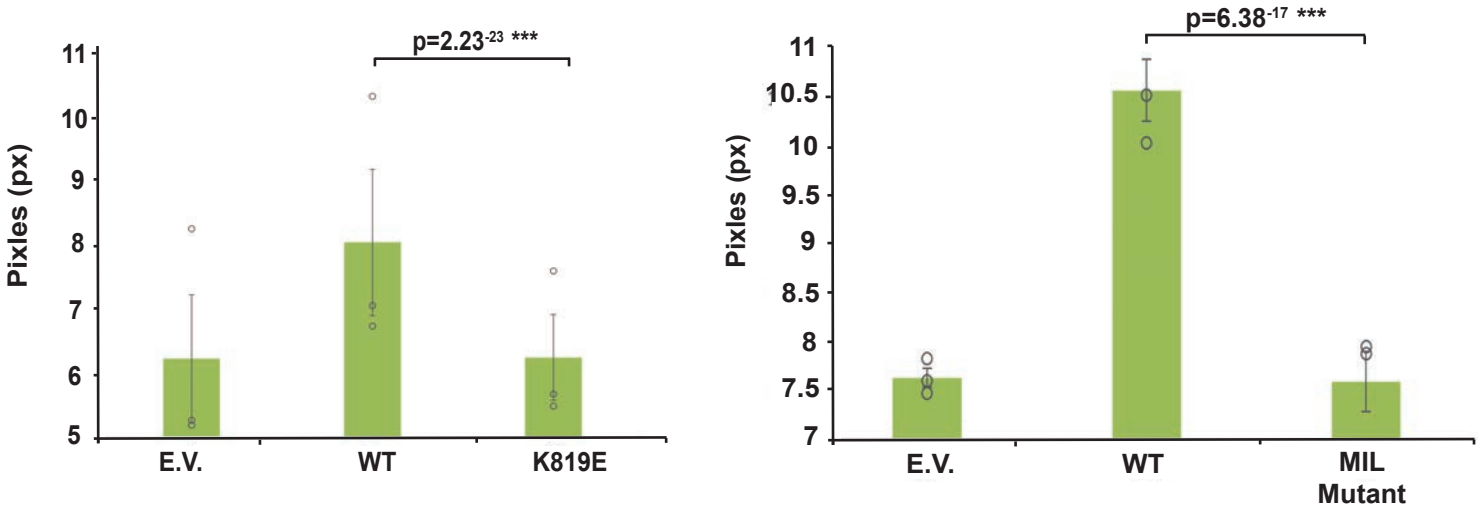
Average Major Axis Length
p=2.23-23 ***
Pixles (px)
11
10
9
8
7
6
5
E.V.
WT
K819E
p=6.38-17 ***
Pixles (px)
11
10.5
10
9.5
9
8.5
8
7.5
7
E.V.
WT
MIL Mutant

b

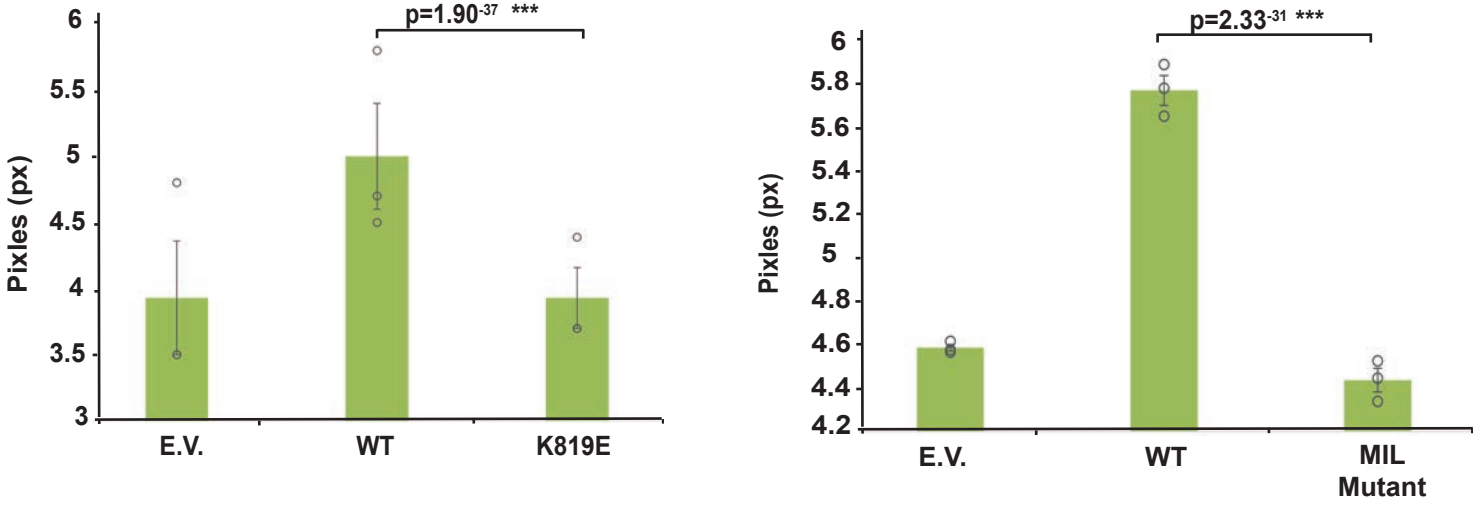
Average Branch Length
p=1.90-37 ***
Pixles (px)
6
5.5
5
4.5
4
3.5
3
E.V.
WT
K819E
p=2.33-31 ***
Pixles (px)
6
5.8
5.6
5.4
5.2
5
4.8
4.6
4.4
4.2
E.V.
WT
MIL Mutant

c

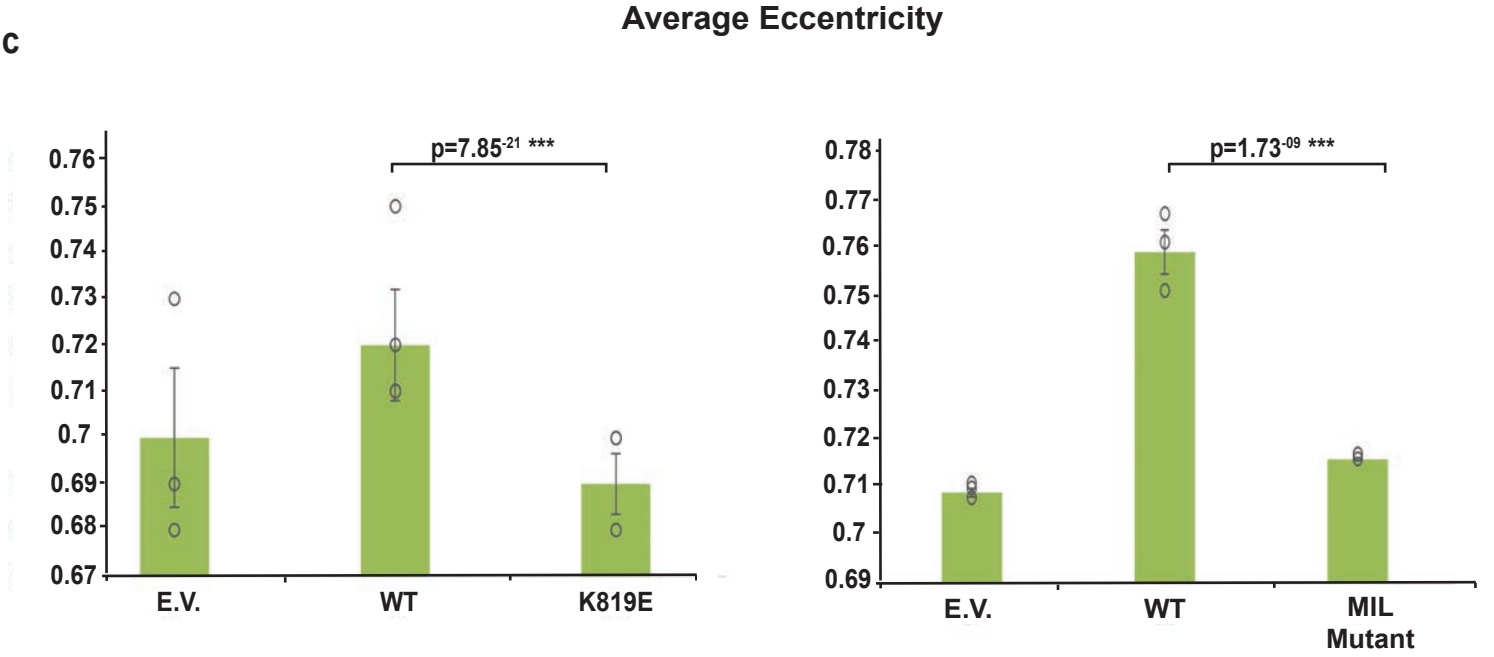
Average Eccentricity
p=7.85-21 ***
0.76
0.75
0.74
0.73
0.72
0.71
0.7
0.69
0.68
0.67
E.V.
WT
K819E
p=1.73-09 ***
0.78
0.77
0.76
0.75
0.74
0.73
0.72
0.71
0.7
0.69
E.V.
WT
MIL Mutant

Supplementary Figure 5. Analysis of the mitochondrial network in HeLa cells expressing WT OPA1 or the indicated mutants using the automated MitoSegNet program. Comparison of mitochondrial fragments, specifically looking at average major axis length, average eccentricity and average branch length, of OPA1 siRNA E.V., WT, membrane-inserting loop (MIL) mutant, and K819E using the MitoSegNet python program. **a,** The major axis length is the length of the object (fragment) identified in the segmented images that correspond to the longest distance from one end to the other of the object and averaged across the sample. **b,** Branch length is the length of each branch identified in the segmented image and averaged across the sample. **c,** Eccentricity is the ratio of the focal distance over the length of the major axis making the value zero a perfect circle. *$p < 0.05$, **$p < 0.01$, ***$p < 0.001$ using an independent two-sample T-test and a Mann-Whitney U-test. N = 219 for each sample over three experimental replicates. Data points represent average percentage of cells across three experimental replicates. Error bars indicate s.e.m.

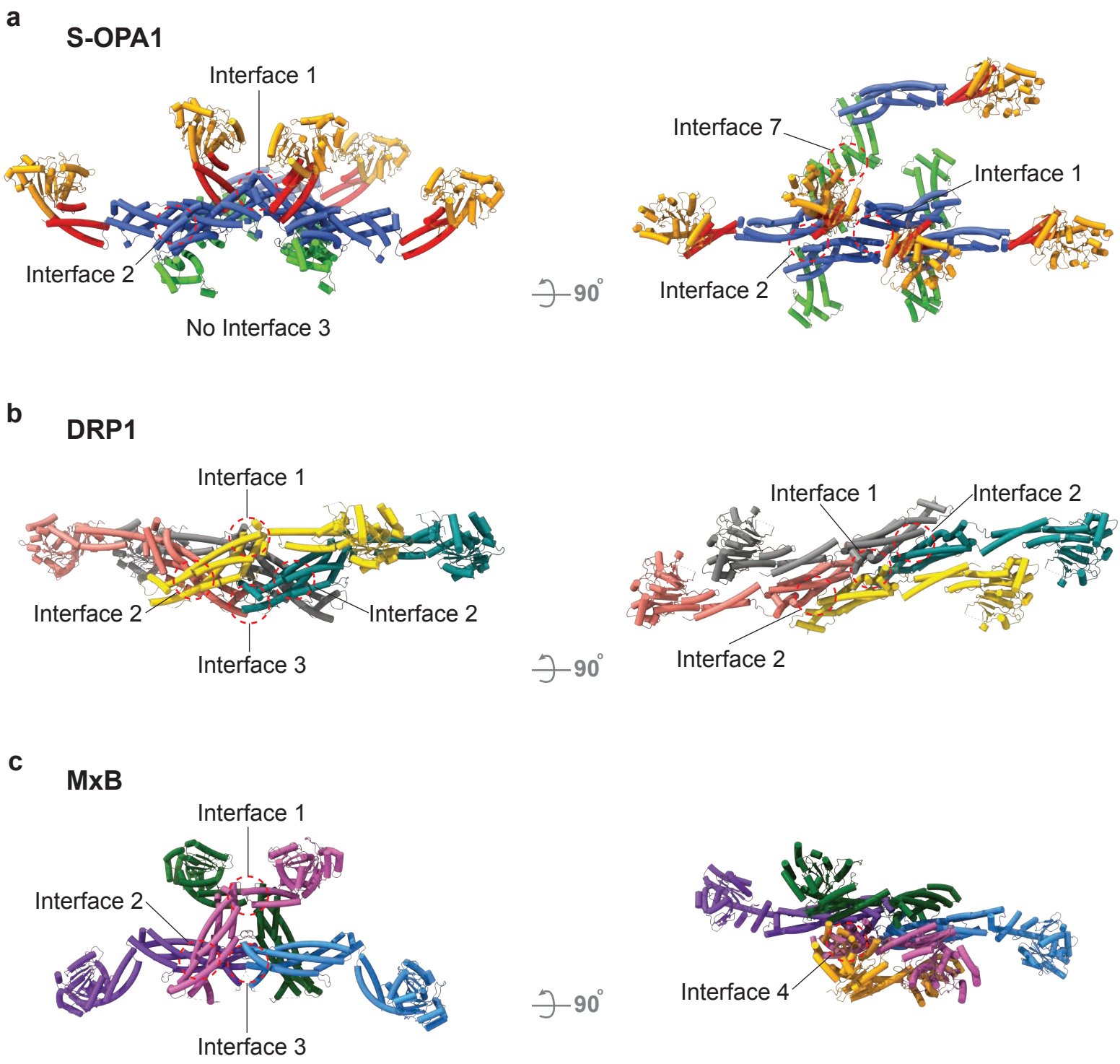

Supplementary Figure 6. Novel interface 7 found within the human OPA1 polymer. a, The structure of S-OPA1 polymer reveals a seventh interface novel to dynamin-related proteins. S-OPA1 contains both interfaces 1 and 2 but lacks interface 3. **b,** Dynamin-related protein 1 (DRP1; PDB ID: 5WP9) contains interfaces 1 through 3. **c,** CryoEM structure of MxB helical assembly (PDB ID: 5UOT) exhibits a fourth inter-molecular oligomerization interface between the GTPase domain and stalk-hinge 1 region. Each interface is highlighted by a red dotted circle for S-OPA1 (**a**), DRP1 (**b**), and MxB (**c**).

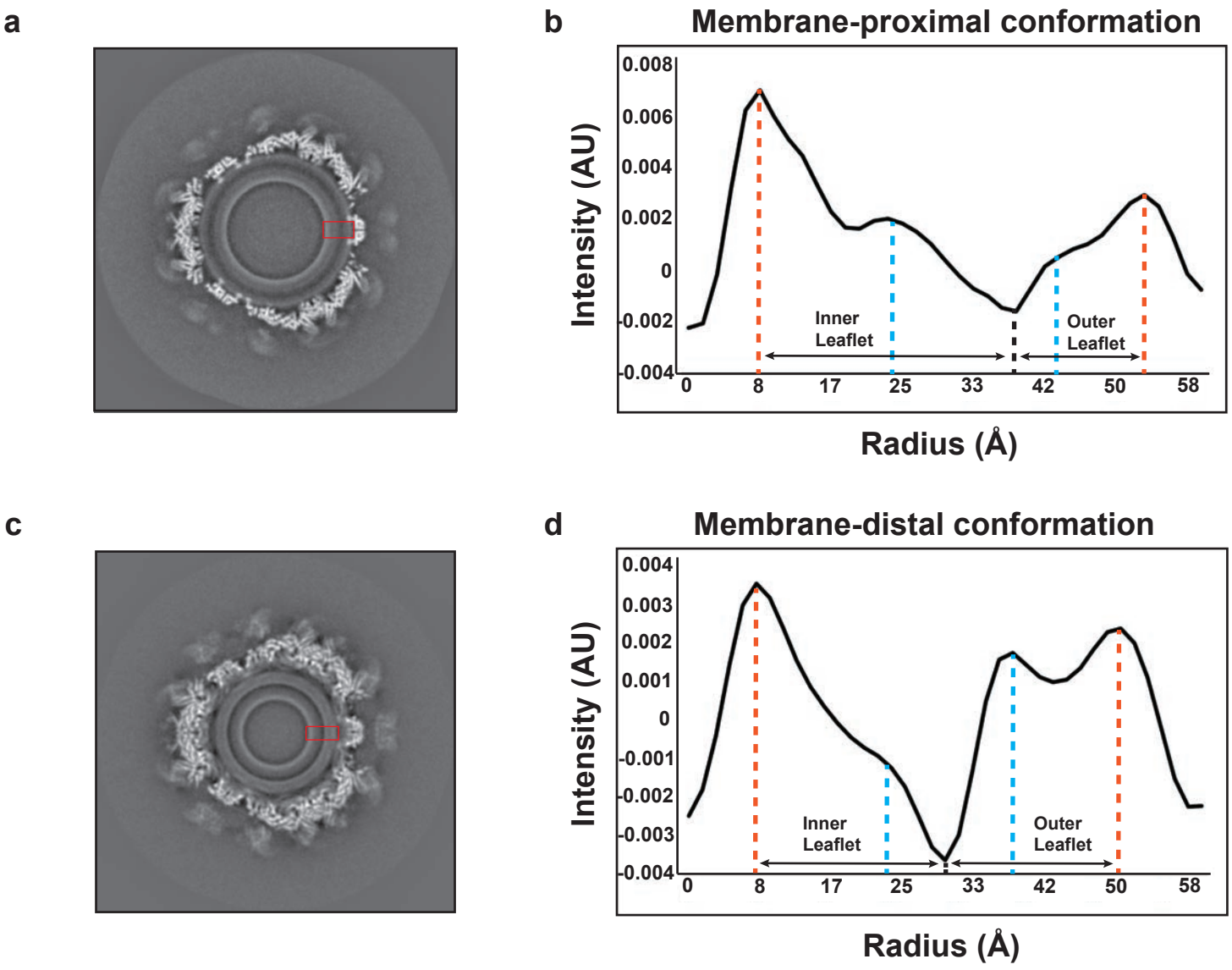

Supplementary Figure 7. Bilayer intensity analysis of membrane-bound S-OPA1 polymers. a, c, Top-down views of grayscale central slices of the reconstructions. Red boxes indicate the region used for intensity analysis. **b, d,** Intensity profiles of each leaflet of the lipid bilayers quantified from cryoEM reconstructions of membrane-proximal and membrane-distal conformations. Black dashed lines mark the inner and outer leaflet boundaries, and orange and blue dashed lines indicate the peaks corresponding to lipid head groups and tails, respectively.

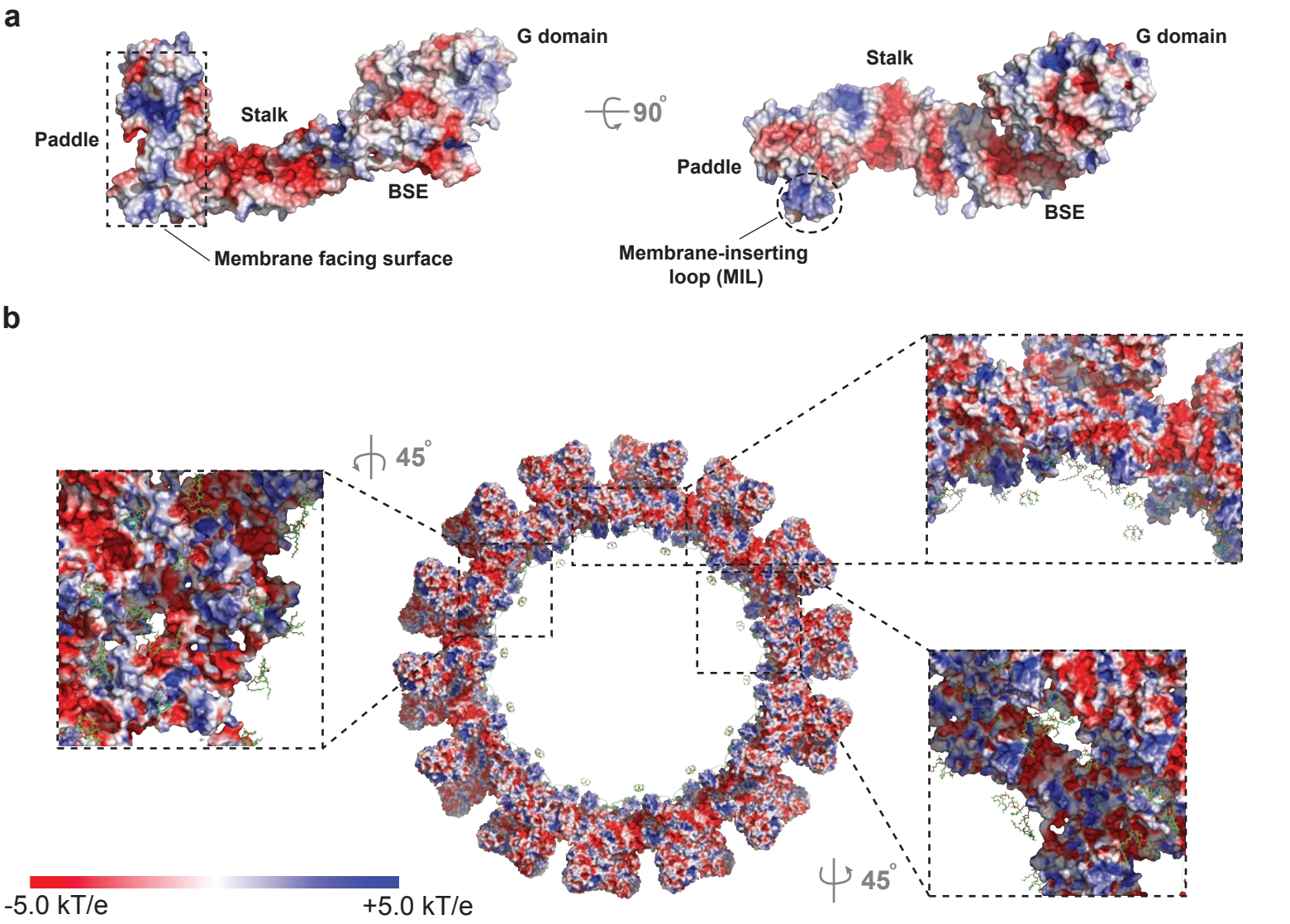

Supplementary Figure 8. Cardiolipin binding by the human S-OPA1 polymer. a, Membrane facing surface of the S-OPA1 paddle domain contains patches of basic residues. The molecular surface is colored according to the electrostatic potential calculated with APBS. **b,** Surface electrostatic potential view of S-OPA1 polymer, showing its positively charged membrane facing surfaces are interacting with cardiolipin molecules (green) extracted from the lipid bilayer. The cardiolipin molecules are interacting with two different positively charged surfaces within the paddle domain and another region near BSE. Inset, close-up views of selected regions involved in cardiolipin binding. Electrostatic potential from -5 to +5 kT/e mapped onto the surfaces of monomeric and polymeric S-OPA1 is shown in different orientations. The surface electrostatic potential is color-coded as indicated by the scale bar.

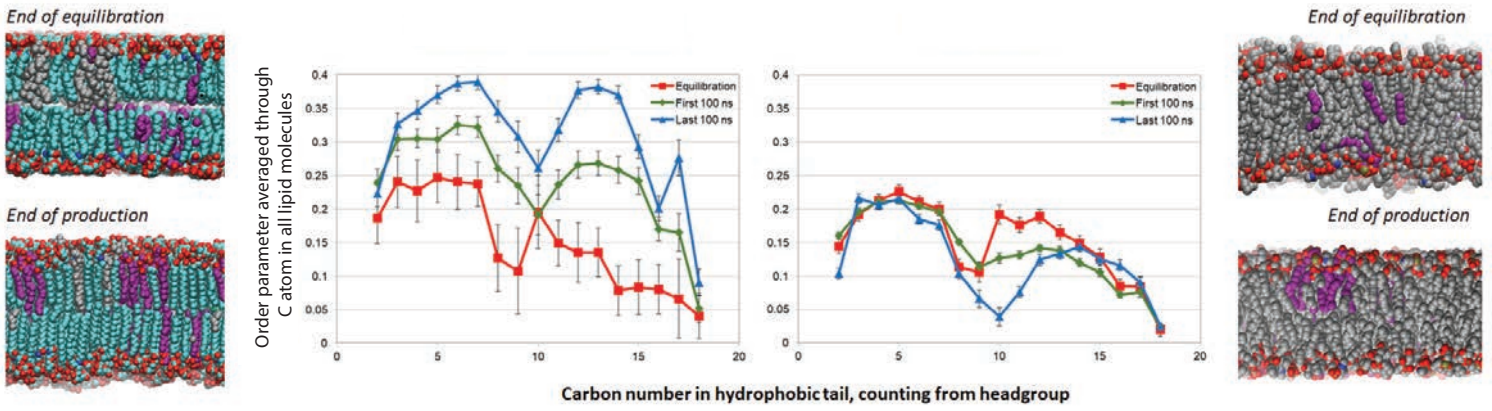

Supplementary Figure 9. The comparison of the GalCer-CL and POPC-CL lipid bilayer stabilities by using atomistic Molecular Dynamics (MD) simulations. a, b, Order parameters for C atoms of lipid tails was determined by using 1.1 μs long atomistic MD simulations of membrane patches of GalCer-CL (a) and POPC-CL (b) lipids and used as a probe of membrane fluidity. The plots show the order parameters for each C atom of the hydrophobic tails averaged across three independent simulations throughout all lipid molecules for the equilibration phase (5 ns, red), the beginning of production sampling (green, first 100 ns of production sampling right after equilibration), and the end of production sampling (blue, last 100 ns of production). Error bars, s.d. The disorder present in the starting system of GalCer-CL membranes is rapidly lost when the system is left to evolve under no bias, resulting in increased order parameters already in the first 100 ns of production simulation (**a**). In contrary, the simulations demonstrate that the disorder of the starting system persists in the system of POPC-CL membranes, indicating high intrinsic fluidity at the simulation temperature of 303 K (**b**). Each lipid is color coded: GalCer (cyan), CL (magenta), and POPC (gray).

Supplementary Table 1 | List of primers used in cell-based assays

pcDNA3-mCherry FWD	actgtgctggatatctgcagatggtgagcaagggcgag
pcDNA3-mCherry-NLS REV	ccactagtccagtgtggtggttagtctagtttaacgcgtttggcagcaggcttgtacagc tcgtccatg
siRNA res. A FWD	ccaaaaagacttttgatcagtggaaagatatgataccagatttgtccgaatataaatg gattgtgcctgacattgtgtgggaaa
siRNA res. A REV	tttcccacacaatgtcaggcacaatccatttatattcggacaaatctggtatcatatcttt ccactgatcaaaagtctttttgg
siRNA res. B FWD	agtggaaagatatgataccagatttgtccgagtacaagtggattgtgcctgaca
siRNA res. B REV	tgtcaggcacaatccacttgtactcggacaaatctggtatcatatctttccact
OPA1 MIL mutant deletion FWD	gaaaacatggtgggtccacaagaacagtgtgttcac
OPA1 MIL mutant deletion REV	gtgaacacactgttcttgtggacccaccatgttttc
OPA1 MIL mutant insertion FWD	gaaaacatggtgggtccagcagctgcagctgcagctgcagctgcagctgcagctg cacaagaacagtgtgttcac
OPA1 MIL mutant insertion REV	gtgaacacactgttcttgtgcagctgcagctgcagctgcagctgcagctgcagctgct ggacccaccatgttttc
OPA1 K738E FWD	ctttggaagaccgatccatatctgatgagcagcaatgggatgc
OPA1 K738E REV	gcatcccattgctgctcatcagatatggatcggtcttccaaag
OPA1 W771A FWD	aaacatggtgggtccagacgcgaaaaagaggtggttatac
OPA1 W771A REV	gtataaccacctctttttcgcgtctggacccaccatgttt
OPA1 W775A FWD	tccagactggaaaaagagggcgttatactggaagaatcgg
OPA1 W775A REV	ccgattcttccagtataacgccctctttttccagtctgga
OPA1 L776A FWD	agactggaaaaagaggtgggcatactggaagaatcggacc
OPA1 L776A REV	ggtccgattcttccagtatgcccacctctttttccagtct
OPA1 K779E FWD	agaggtggttatactgggagaatcggacccaagaa
OPA1 K779E REV	ttcttgggtccgattctcccagtataaccacctct
OPA1 R781E FWD	gaggtggttatactggaagaatgagacccaagaacagtgtg
OPA1 R781E REV	cacactgttcttgggtctcattcttccagtataaccacctc
OPA1 K819E FWD	aaataaccacagtccgggagaaccttgaatcccga
OPA1 K819E REV	tcgggattcaaggttctcccggactgtggttattt
OPA1 R824E FWD	gtccggaagaaccttgaatccgagggagtagaagtagatccaagc
OPA1 R824E REV	gcttggatctacttctactccctcggattcaaggttcttccggac
OPA1 R858E FWD	aaacagctctaaaccattgtaacctttgtcgagagggtttttattactaccaaaggc
OPA1 R858E REV	gcctttggtagtaataaaaaccctctcgacaaaggttacaatggtttagagctgttt
OPA1 H866A FWD	aagaggtttttattactaccaaagggcttttgtagattctgagttggaatgc
OPA1 H866A REV	gcattccaactcagaatctacaaaagccctttggtagtaataaaaacctctt